Electron Energy Loss Spectroscopy assessment of cationic migration in $La_{2/3}Ca_{1/3}MnO_3$ thin films

Sònia Estradé Albiol

Directors of Master's Thesis: Dr. Francesca Peiró i Martínez and Dr. Jordi Arbiol i Cobos

Departament d'Electrònica, Universitat de Barcelona,
Martí i Franquès, 1, 08028 Barcelona
Ph: 34 93 4032 39 47; Fax: 34 93 402 11 48; e-mail: sestrade@el.ub.es

In the present work Transmission Electron Microscopy (TEM) and Electron Energy Loss Spectroscopy (EELS) are applied for the evaluation of trivalent cationic migration in epitaxial thin films of $La_{2/3}Ca_{1/3}MnO_3$ (LCMO). The first part of the work shows the comparative results of the growth by RF-sputtering of both annealed and as grown $La_{2/3}Ca_{1/3}MnO_3$ (LCMO) layers of various thicknesses on (001) $LaAlO_3$ (LAO) substrates. Lanthanum diffusion is detected for LCMO films grown on LAO as a function of annealing and layer thickness and is determined to play a major role in the degradation of the magnetic properties found in this system. In the second part, thin LCMO layers simultaneously grown, also by RF-sputtering, on (001) and (110) $SrTiO_3$ (STO) are evaluated. La diffusion is also found in thin LCMO films grown on STO and the correlation with magnetic properties depending on the film thickness is discussed.

04. Materials for spintronics: manganites, EELS, TEM.

I. INTRODUCTION

Magnetic tunnel junctions (MTJ) are considered of great interest because of their potential application to magnetic memory devices[1,2]. Doped manganites presenting colossal magnetoresistivity seem to be excellent candidates to implement such devices. Nevertheless, it has been reported that these thin layer materials used in MTJs yield Curie temperature values clearly bellow those corresponding to bulk material [3,4,5,6], which behaviour depends as well on the growth direction of the layers[6].

The origin of this strong degradation of magnetotransport properties with temperature is not well understood yet. Plastic strain relaxation due to the substrate/film mismatching has been suggested as a possible cause of this degradation. It has been stated that doped manganites subjected to different lattice mismatch figures when being grown on different substrates present a different defect density, samples with the least amount of defects exhibiting best magnetic properties[5,7]. Therefore, different substrates as $LaAlO_3$ (LAO) or $SrTiO_3$ (STO) have been used in order to tailor the strain conditions: whereas LCMO grows on STO under tensile strain (≈+1.2 %) allowing to get a defect-free epitaxy, LCMO grows on LAO under compressive strain (≈-1.8 %), leading to a 3D growth process with misfit dislocations and twins, and depressed magnetic properties[5,7].

Less attention has been paid to the influence of other physical phenomena besides microstructural defects in order to explain the magnetic properties of thin LCMO films. Nevertheless, it has also been reported that chemical segregation in the doped manganite films leads to depressed magnetic properties[3].

And last but no least, whilst thicker films have been studied in detail[3,4], not much effort has been paid to the structure and chemical homogeneity of very thin films of doped manganites, with thickness under 15 nm, which may give further insight into the growth mechanisms and substrate-induced phenomena in such materials.

Therefore, a correlation of the microstructural and chemical analysis of doped manganite thin films is of the greatest importance in order to understand how strain due to lattice parameter mismatch, plastic relaxation of deformations, and deviations from stoichiometry through interdiffusion or segregation of the species at the heterostructure interface affect macroscopic magnetic behaviour.

In this work, after a brief introduction to Electron Energy Loss Spectroscopy (section II) we present the detailed structural and chemical characterization of as-grown and annealed LCMO films grown on (001) LAO substrates (section III), as well as the comparative results of very thin LCMO films simultaneously grown on (001) STO and (110) substrates (section IV). In both cases La diffusion towards the top of the layer has been detected and the correlation with the magnetic properties of the epitaxial layers is discussed.

II. ELECTRON ENERGY LOSS SPECTROSCOPY IN A TRANSMISSION ELECTRON MICROSOCOPY

In the Transmission Electron Microscope (TEM), electrons cross through the specimen. In this process they may not undergo any scattering process (direct beam), or suffer elastic scattering (e- scattered by the atomic nuclei), or inelastic scattering. The direct beam is used in Bright Field Image, whereas elastic scattering gives rise to electron diffraction, dark field image and Z-contrast image. Inelastic scattering is an electron-electron process, in which one incident fast electron gives a part of its energy to one sample electron (or a collective state of the sample electrons). Many physical phenomena can be studied when an incident electron inelastically interacts with the sample: secondary electrons, de-excitation photons, etc. In particular, Electron Energy Loss Spectroscopy (EELS) [8,9] is the study of the fast electrons once they have crossed the sample. Notice that the main contribution will be due to electrons that have not undergone any inelastic scattering –zero loss.

Physically, in an inelastic scattering event in a crystal, an initial state (atom core state or Bloch wave state) is excited to a final state (a higher energy core state, a Bloch wave state, or even a free state), by getting energy from a primary beam electron $|k>$ which loses energy and becomes $|k'>$; notice that in the general case not only the modulus, but also the direction of the electron momentum will be changed. As in an EELS experiment we want to know how many electrons have lost what amount of energy, a prism is used that discriminates the energy of every transmitted electron. The electronic optics of such devices can be extremely complicated but the physical idea is as simple as to use a magnetic prism. In the magnetic prism there is a magnetic field *B* perpendicular to the travelling direction of the electrons; under field B the electrons will start to travel in a circular orbit with a radius depending on the electron mass m_e, its charge and the velocity of the electron. Notice that an electron accelerated at some hundreds of keVs will be subjected to relativistic effects. At the end of the prism, a detector can be used, which can give an answer to our primary question: how many electrons have lost what amount of energy, and, thus, we get an EELS spectrum (energy versus counts –i.e.: electrons). In this EELS spectrum one can see different relevant features. The **zero-loss peak**, corresponds to those electrons that have not undergone an inelastic scattering, and its width in the energy scale is a figure of merit of the precision of the experiment; it is possible under favourable conditions to observe excitations of **valence electrons** to free states; the **plasmon excitations** correspond to the strong collective excitations of the valence electrons; finally, **core-loss peaks** correspond to excitations from core states of atoms in the sample. These peaks are generally identified by direct comparison with a reference table. Once the peaks have been identified, one can try to quantify them. In general, the relative concentration of two elements is proportional to the rate of the areas of both their peaks, the proportionality constant being a function of the studied elements, the compound they are in and the experimental conditions of the microscope.

Furthermore, the comparison of two peaks corresponding to different transitions of the same element, or the energy shift (typically a few nanometers away from the tabulated value) of a given peak, may carry relevant information about the electronic state of the studied element. In this sense, one of the goals of the present work has been the measurement of Mn L_3 peak edge and of Mn L_3 / Mn L_2 peak intensity ratio by the implementation of a home-made program ("ManganitaS") that performs recalibration of the energy axis as well as background and continuum subtraction, peak onset estimation and integration of fitted Gaussian curves for both Mn L_3 and Mn L_2 peaks. Integration ranges have been chosen by the quantification of LCMO reference bulk samples with controlled stoichiometry.

Finally, as far as thin foil preparation is concerned, the samples, were prepared in cross section geometry by flat polishing down to 50 µm, followed by a dimpling down to 25 µm and a final Ar+ bombardment at V=5kV with an incident angle of 7° using a PIPS-Gatan equipment. High resolution TEM (HRTEM) has been carried out in a Jeol 2010F microscope, with field emission gun, operating at 200 keV. EELS spectra have been obtained with a Gatan Image Filter (GIF) spectrometer.

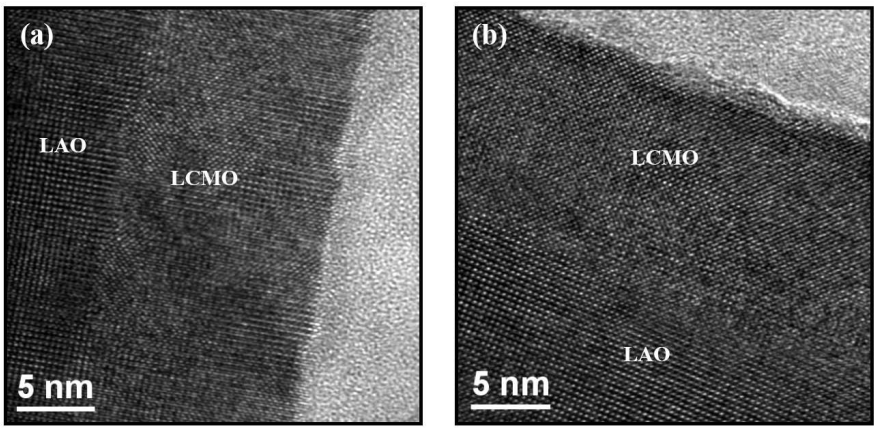

Fig. 1. High resolution images of as grown (a) and annealed (b) 14 nm thick samples along [100] zone axis.

TABLE I
LATTICE PARAMETERS OF STUDIED SAMPLES DETERMINED BY TEM AND XRD

	c [Å] determined by TEM		*c [Å] determined by XRD*		a [Å] determined by TEM		*a [Å] determined by XRD*	
thickness	As grown	Annealed	*As grown*	*Annealed*	As grown	Annealed	*As grown*	*Annealed*
14 nm	3.94	3.88	*3.957*	*3.878*	3.82	3.83	*3,793*	*3.865*
48 nm	3.91	3.85	*3.920*	*3.868*	3.82	3.88	*3,793*	*3.857*
90 nm	-	3.85	*3.897*	*3.870*	-	3.86	*3,820*	*3.853*

III. LA SEGREGATION IN THIN $La_{2/3}Ca_{1/3}MnO_3$ FILMS GROWN ON $LaAlO_3$ (001) SUBSTRATES

A. Experimental

In this first part of the work, we will show the comparative results of the RF-sputtering growth of LCMO layers of various thicknesses on (001) LAO depending on both thickness and annealing treatment. Whereas depressed magnetic behaviour in LCMO/LAO systems is currently understood in terms of microstructural defects, our results indicate that, in the case of thin, stressed, defect-free LCMO films grown on LAO, in which Curie Temperature is well below that of bulk material, some other phenomena leading to a poorer magnetic performance in LCMO/LAO systems must be taken into account as well.

LCMO layers have been grown by RF-sputtering on (001) LAO substrates, with nominal thicknesses ranging from 14 to 93 nm (table I), at a deposition temperature of 800ºC, a deposition pressure of 330mtorr, and an O_2/Ar pressure ratio of 1/4; afterwards, they have been submitted to an in situ annealing process in an O_2 atmosphere at a pressure of 350torr and at a temperature of 800ºC for 60 minutes; every such sample has been annealed at 1000ºC, also keeping an as grown sample for comparison[10].

The structures have been characterized by high resolution electron microscopy (HRTEM) and electron energy loss spectroscopy (EELS), paying special attention to the determination of the quality of the LCMO/LAO interfaces, and to the compositional homogeneity of the layers.

B. Results

Figure 1 displays HREM images of as grown (a) and annealed (b) 14 nm thick samples along [100] zone axis. Abrupt, flat and homogeneous interfaces between LCMO film and LAO substrate and LCMO free surfaces have been found in the thinnest as-grown samples. On the other hand, interfaces between LCMO film and LAO substrate and LCMO free surfaces have been found to get slightly rougher as layer thickness increases and with the annealing treatment. The layers have been determined to be homogeneous and defect-free at least in the studied region, with mosaicity increasing again with thickness and after annealing treatments.

The LCMO(001)[100]//LAO(001)[100] epitaxial relationship has been confirmed by fast Fourier transform (FFT) of high resolution images of layer and substrate, for all studied samples. High resolution images have also been studied by Gaussian fitting of intensities corresponding to atomic columns, as to locate their relative positions with high precision[11]; this method has been used to determine lattice parameters instead of FFT, in good agreement with those found by XRD (table I); c parameter decreases, and a parameter increases, with annealing and with thickness towards bulk value, as in plain stress gradually relaxes with thickness and when annealed.

Moving towards EELS analysis, first of all general spectra (between 325 and 870 eV) have been acquired throughout the sample along a direction perpendicular to the interface following the evolution from the substrate to the free surface of the layer. The Ca/La ratio relative evolutions in the LCMO layers have been estimated from the general spectra by intensity integration of the Ca and La peaks and are displayed in figure 2, normalised to the ratios near the interface. In all cases, a cationic segregation process leading to an increase of the La content while approaching film surface has been detected, whilst the Ca/La variation rate slows down with annealing process and/or by increasing sample thickness.

EELS spectra in the energy loss range between 500 and 675 eV (in which range the Mn $L_{2,3}$ peaks -640, 651 eV- and the O K peak -532eV- can be found) have also been obtained. From this point on, sequential acquisition at different distances from the interface has been carried out. An example of the whole set of acquired spectra, corresponding to the as grown, 14 nm thick sample, is displayed in figure 3. A change in Mn L_3 peak onset position, and in Mn L_3 to Mn L_2 intensity ratio, with position is hinted in figure 3.

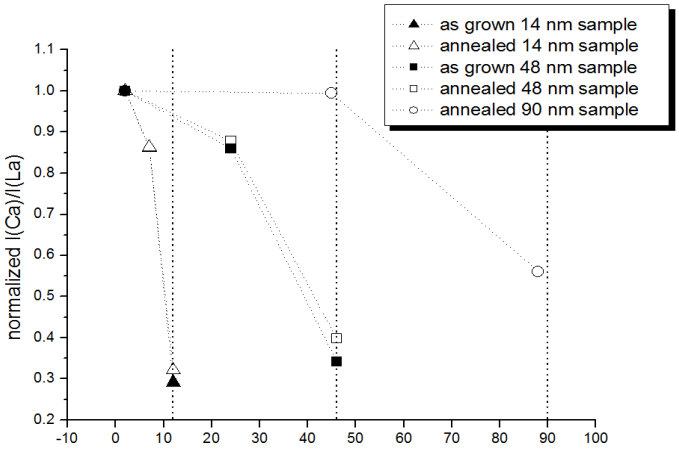

Fig. 2. La/Ca relative intensity variation along LCMO layers.

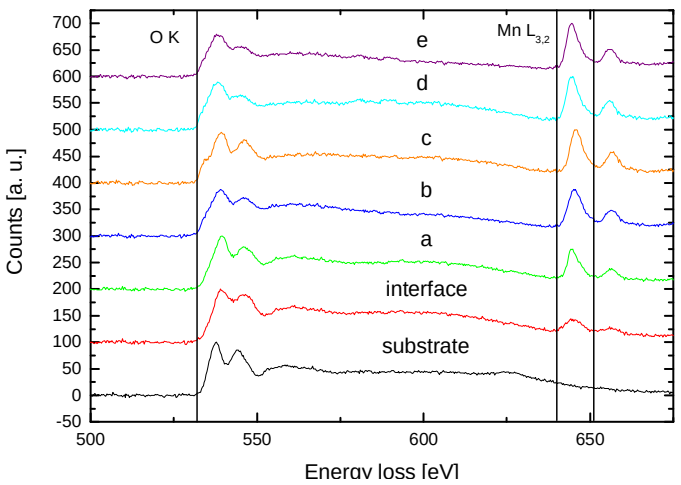

Fig. 3. Evolution of the EELS spectra, in the electron energy loss range between 500 and 675 eV, obtained in several points of the layer as a function of the distance to the interface for an as grown 14 nm thick sample.

Mn oxidation state determination by means of EELS has been widely reported [12,13,14,15,16,17]. In our case, the measurement of peak edge and Mn L_3 to Mn L_2 ratio have been determined by the home-made program ("ManganitaS") in Matlab software that performs recalibration of the energy axis, background and continuum subtraction, peak onset estimation and integration of fitted Gaussian curves for both Mn L_3 to Mn L_2. The experimental results are illustrated in figure 4 together with the theoretical values found in literature[14,16,17] for the Mn oxidation states 2+, 3+ and 4+. The most relevant feature in figure 4 is a shift towards lower energies of the Mn $L_{2,3}$ peaks as well as a variation of the intensity ratio of these two peaks as the distance to the interface is increased. According to the data corresponding to the bulk reference samples, these observations imply that the Mn oxidation state would significantly change along the layer thickness. Even more, this variation of the Mn oxidation state is also compatible with the detected La diffusion towards the free surface of the films, as suggested by the observed variation of the La/Ca ratio, more pronounced for thinner and as-grown samples.

C. Discussion

As previously mentioned LCMO on LAO, grows under compressive strain (≈-1.8 %) leading to an increase of the out-of-plane parameter, c. This elongation of the unit cell along the c axis induces an easy magnetization axis perpendicular to the film plane. The departure of the easy magnetization axis from perpendicular to film plane to parallel to plane has been observed as structural strain relaxes by increasing film thickness or by high temperature annealing processes[18]. In our samples, both saturation magnetization M_S, and T_C exhibit a clear dependence on sample thickness (see Fig. 5 and 6). In this figures we also show that the high temperature annealing process substantially improves magnetic properties and this improvement is notoriously stronger in thinner samples. At first sight this evolution of T_C and M_S can thus be correlated with variations of structural strain, nevertheless as pointed out

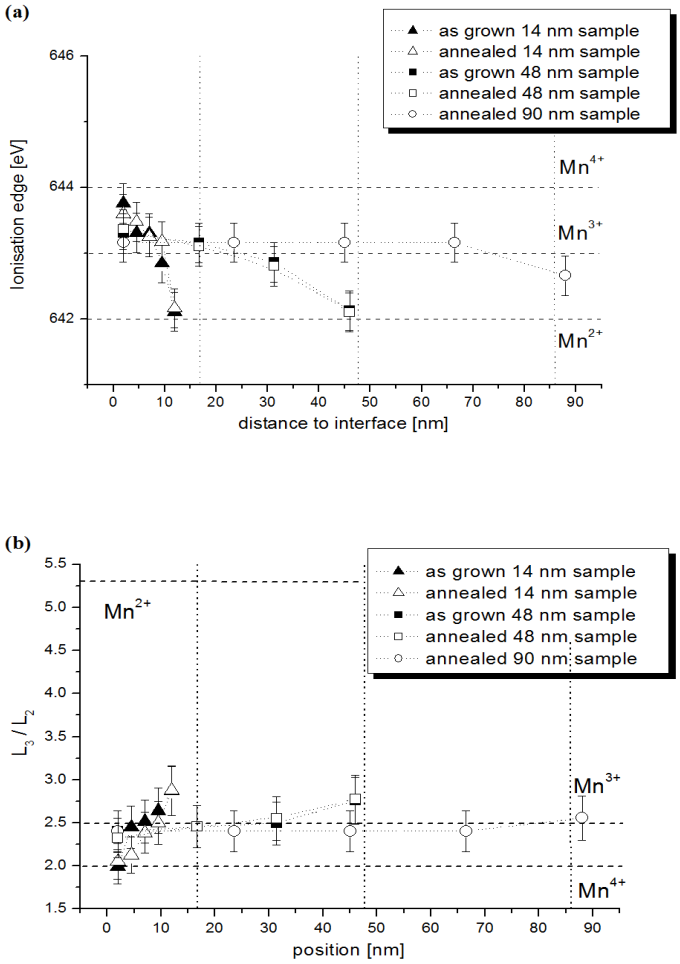

Fig. 4. Ionisation edge variation –all data affected by a 10% relative error- (a) and relative intensity variation –all data affected by a 5% relative error- (b) of the Mn L3 and L2 peaks along LCMO layers.

by A. Biswas et al[19] the LCMO/LAO system exhibits a 3D growth mechanism from the early stages leading to a granular character of the films and making it very difficult to obtain a homogeneously strained film. On the other hand in-plane biaxial compression, as in LCMO/LAO system, should imply an expansion of the out-of-plane parameter because of the Poisson effect leading to a flatten of the Mn-O-Mn angle thus, promoting a reduction of the Jahn-Teller effect and the increase of T_C [20] which is not observed in our case. Therefore, we should conclude that structural strain alone cannot account for the variations of T_C and M_S.

Interestingly enough, the observed evolution of T_C and M_S clearly correlates with the segregation process of La ions towards the surface of the films. The formation of a La floating layer during LCMO thin film growth should lead to the appearance of a La-enriched layer of few nm close to the free surface of the films. This layer should exhibit strongly depressed magnetic properties in agreement with the existence of a surface magnetic dead layer as detected from magnetic measurements in LCMO/LAO thin films[21]. Since this La-rich layer is very thin (few nm) its effects are negligible for thick samples but critical for thin ones. This La segregation process

would, in turn, imply a departure from the nominal composition (2/3-1/3) $Mn^{3+/4+}$ valence balance, thus becoming an efficient mechanism for the reduction of T_C and M_S. Nevertheless, concerning the driving mechanism for La segregation, it should be mentioned that strain may be at the origin of this cationic migration since a way to accommodate structural strain in thin films could be by means of the segregation of ions with larger or smaller size. Therefore, elastic strain accommodation in LCMO films grown on STO (tensile strain of about 1.1%) occurs by 2+ valence cationic migration[3]. In contrast, under compressive strain, as in LCMO/LAO (-1.8%), a 3+ valence cationic migration towards film surface should be expected, since La^{3+} ionic radius (1.36 Å) is higher than Ca^{2+} ionic radius (1.34 Å). On the other hand, high temperature annealing processes would promote rediffusion of La ions in the whole film which would moderate the effect of the cationic migration (see Fig. 4 and Fig. 5) and substantially improve both T_C and M_S as observed.

In the past, depressed magnetic behavior in LCMO thin films grown on LAO had been usually explained in terms of the presence of microstructural defects [5,7]. In the present work we have shown that a local La diffusion can lead to a significant decreasing in magnetic performance in thin, stressed, defect-free LCMO films.

IV. LA MIGRATION TOWARDS FREE SURFACE OF THIN $LA_{2/3}CA_{1/3}MNO_3$ LAYERS GROWN ON $SRTIO_3$ (001) AND (110) SUBSTRATES

A. Experimental

In this second part of the work we give the comparative results of the simultaneous growth by RF-sputtering of LCMO thin layers on STO (001) and (110) substrates by TEM and EELS. For (001) STO, in plane [100] and [010] directions are equivalent and neutral SrO or TiO2 terminating surfaces are possible[22]. On the contrary, for (110) STO, in plane [001] and [1-10] directions are non equivalent, and terminating layers are polar, either +4 ($La_{2/3}Ca_{1/3}MnO$) or -4 (O_2).

LCMO layers have been grown simultaneously on STO substrates in the considered orientations, (001) and (110), by RF-sputtering, at a RF power of 15W, a target-substrate distance of 6 cm, a deposition temperature of 800ºC, at a pressure of 330mtorr, with a O_2/Ar pressure ratio of 1/4 and a growth rate of 0.12 nm/min; afterwards, they have been submitted to an annealing process in an O_2 atmosphere at a pressure of 350torr and at a temperature of 800ºC, and heated to 1000ºC for two hours[6].

B. Results

Previous structural and magnetic characterization was carried out on a wide range of layer thickness from 8nm up to 150 nm[23]. The interplanar distances as a function of layer thickness for both orientations have been determined by XRD (figure 7). XRD results indicate that for (001) orientation there is only a slight relaxation of in-plane parameter d_{100} whilst for (110) orientation, a gradual and anisotropical relaxation for both in-plane d_{001} and $d_{1\text{-}10}$ is found, with a faster in-plane d_{001} and $d_{1\text{-}10}$ relaxation than for in-plane d_{100} in (001) films. Out-of-plane parameters contract for thin films and then, over a critical thickness, tc (about 15nm), expand again for both samples, towards bulk value for (110) sample, and always well bellow bulk value for (001) sample. For both (001) and (110) films, the out-of-plane cell parameters in thin foils (t<tc) are substantially larger than expected.

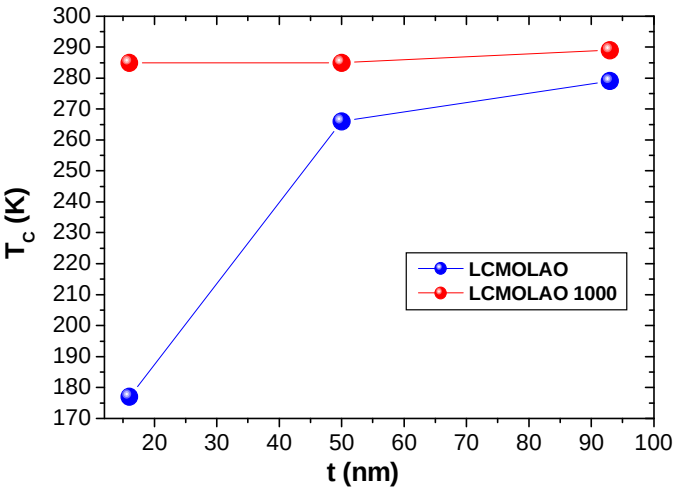

Fig. 5. Tc value as a function of layer thickness for annealed and as grown samples.

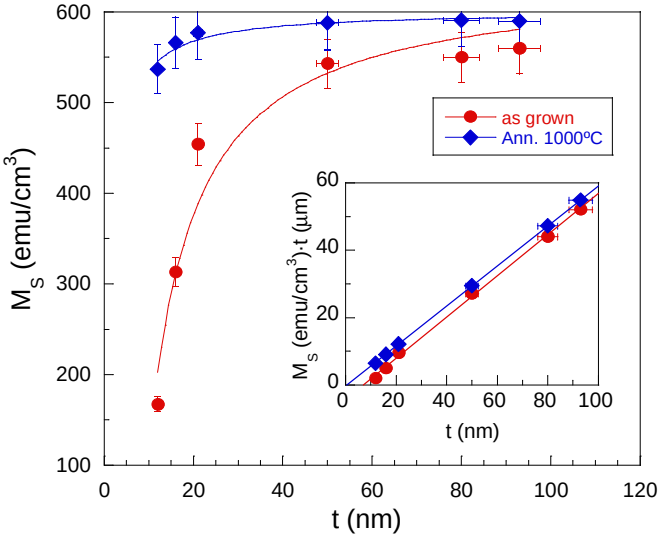

Fig. 6. Saturation magnetisation as a function of layer thickness for as-grown and annealed samples

When calculating the unit-cell volumes from the measured interplanar distances these volumes are always over that of bulk LCMO. Upon increasing thickness, there is a gradual compression of the cell volume, more pronounced for the (110) films. There is an anomalous unit-cell volume expansion for (001) and (110) films for low thicknesses t<tc, again more pronounced for (110) films, corresponding also with the dashed area in low thickness range in figure 7.

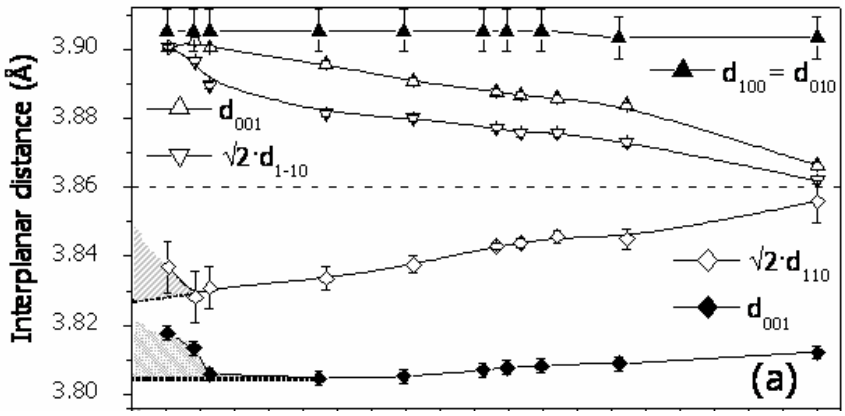

Fig. 7. Interplanar distance as a function of layer thickness in LCMO films grown on STO (001) (filled symbols) and STO (110) (blank symbols).

To gain further insight into the anomalous evolution of both lattice parameters and unit cell volume in the range of low thicknesses, very thin samples grown on both (001) and (110) STO substrates have been studied by Transmission Electron Microscopy. The sample grown on (001) STO substrate exhibits the expected LCMO(001)[100]//STO(001)[100] epitaxial relationship and the layer thickness has been determined to be 8.4 nm. The high resolution XTEM image along the [110] zone axis (figure 8a) exhibits abrupt interfaces and no evidence of misfit dislocations has been detected across the examined region. This result is in good agreement with XRD lattice parameters measurements that showed that, for the sample grown on (001) substrate, the layer is completely adapted ($a_{//}$ = 3.91Å; $a_{\perp}$ = 3.82Å). Local variations of the lattice parameters in the growth direction have been estimated by a precise measurement of the position of the intensity maxima along a column in HREM images[11]. No significant deviation form the mean value has been measured along the thin film.

The sample grown on (110) STO substrate presents the expected relationship LCMO(110)[001]// STO(110)[001] with a layer thickness of 10.3 nm. The high resolution images (figure 8b) do not show relevant differences with respect to the sample grown on [001] direction, except for a greater roughness both at the interface and at the free surface of the LCMO layer. In this case there are neither evidence of local variations of lattice parameters of the layer nor misfit dislocations at the interface while the XRD measurements indicated a 5% of strain relaxation ($a_{//}$ = 3.90Å; $a_{\perp}$ = 3.84Å).

Moving towards EELS analysis, first of all general spectra (between 325 and 870 eV) have been obtained in the layer of both [110] and [001] orientation (figure 9). Spectra have been

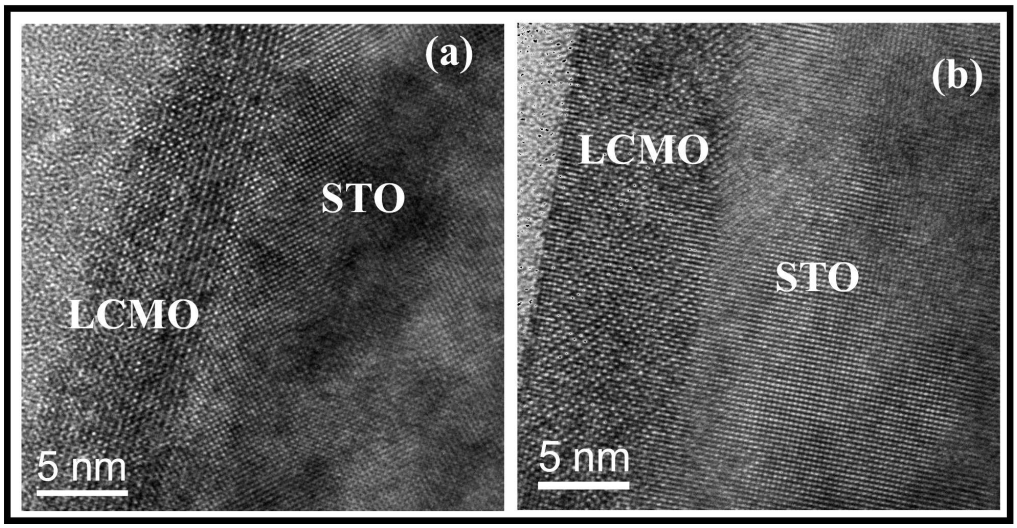

Fig. 8. High resolution image of the interface of the sample grown on (001) STO substrate along [100] zone axis (a) and of the sample grown on (110) STO substrate along [001] zone axis (b).

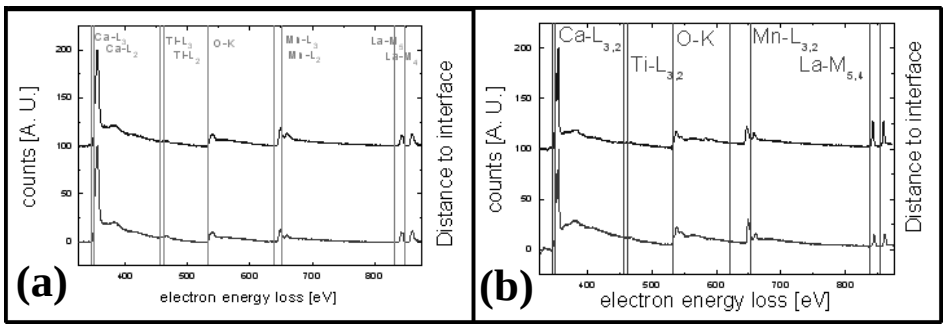

Fig. 9. EELS spectra, in the electron energy loss range between 325 and 870 eV, obtained in two points of the layer at a different distance from the interface for the (001) STO sample (a) and for the (110) STO sample (b).

acquired throughout the sample along a direction perpendicular to the interface following the evolution from the substrate to the free surface of the layer. It is noticeable a variation of the La $M_{5,4}$ peaks intensity in the spectrum corresponding to the layer surface with respect to the spectrum obtained near to the interface, more pronounced for (110) sample (fig. 9b), than for (001) sample (fig. 9a).

The Ca/Mn, La/Mn and O/Mn ratios in the LCMO layers have been estimated from spectra obtained near the interface region and in the top of the layer[24]. The O/Mn ratio variation between these positions is not statistically significant, conversely to those noticed in the Ca/ Mn and La/ Mn ratios. A figure of the relative variation of the Ca/Mn and La/Mn ratios (namely X/Mn ratios) has been calculated as the X/Mn ratio near the interface $(X/Mn)_i$ subtracted to the X/Mn ratio near free surface $(X/Mn)_s$, and then normalizing this subtraction to $(X/Mn)_i$. For (001) sample, Ca/Mn (-3%) and La/Mn (2%) relative variations are under the value of the experimental precision (about 5%), while for (110) sample, Ca/Mn (-26%) and La/Mn (18%) relative variations are relevant.

EELS spectra in the energy loss range between 500 and 675 eV (in which range the Mn $L_{2,3}$ peaks -640, 651 eV- and the O K peak -532eV- can be found) have also been obtained. As the characteristic Sr peak is found at a very high energy, and, thus, the signal/noise ratio is very low, we have determined that the shape (energy loss near edge spectra (ELNES))[8] of the O K peak found in the zones where STO was expected was indeed compatible with this compound. From this point on, sequential acquisition at different distances from the interface has been carried out. The results are presented in figure 10a for (100) sample and 10b for (110) sample.

Mn oxidation state has been determined as shown in previous section by means of the ManganitaS Matlab routine. The experimental results are illustrated in figure 11 together with the theoretical values found in literature [15,16,17] for the Mn oxidation states 2+, 3+ and 4+. The most relevant feature is a shift towards lower energies of the Mn $L_{2,3}$ peaks as well as a variation of the intensity ratio of these two peaks as the distance to the interface is increased, specially for the (110) sample. According to these data in comparison with the references, Mn oxidation state would significantly change along the layer, and especially near free surface for the (110) sample.

C. Discussion

Taking into account a charge balance, a La^{3+} diffusion towards free surface would imply a diminishing of Mn valence state compatible with the observed Mn reduction as approaching the layer surface. However, the mechanism triggering this La diffusion is not understood yet. It has been usually reported that elastic strain accommodation in LCMO films occurs by 2+ valence cation migration in tensile strained films[5]. Conversely, despite the fact that our system presents also tensile strain, we have detected 3+ valence cation migration

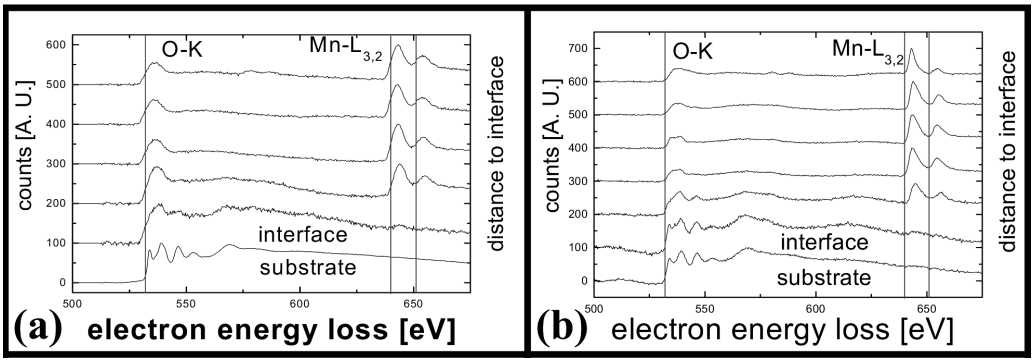

Fig. 10. Evolution of the EELS spectra, in the electron energy loss range between 500 and 675 eV, obtained in several points of the layer as a function of the distance to the interface for (001) STO sample (a) and for (110) STO sample (b).

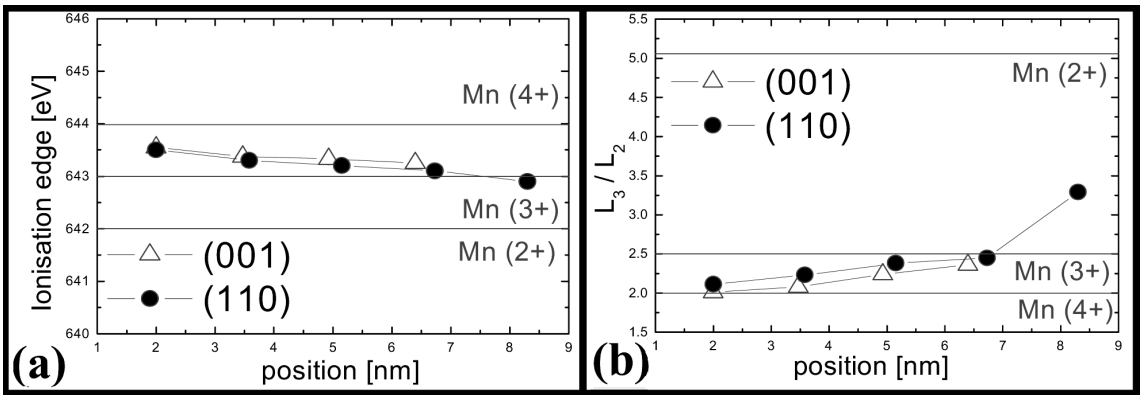

Fig. 11. Ionisation edge variation –all data affected by a 10% relative error- (a) and relative intensity variation –all data affected by a 5% relative error- (b) of the Mn L_3 and L_2 peaks.

towards film surface, in apparent contradiction with an expected segregation of the element with lower covalent radius toward the surface in tensile systems. Therefore tensile strain accommodation does not account for the observed La migration in this system. Other authors have reported an initial La enrichment (Sr concentration decreasing) along the first few nanometers as layer thickness increases when analyzing thick LSMO films[25]. The origin of this La segregation specially at the first stages of growth, might be related to the generation of trivalent cationic vacancies originated when doping manganites with divalent cations.

As far as magnetic measurements for thick layers is concerned, a gradual decreasing of the magnetization as reducing thickness, less pronounced for (110) than for (001) films (figure 12) is detected. (110) LCMO films have higher saturation magnetization and Curie temperature than (001) LCMO films of similar thickness (figures 12b and 12c). Unfortunately, these data have only been obtained for t>tc. Even if they present a good agreement with structural results in this range, where (110) orientation unit cell volume is closer to bulk than that of (001) orientation, for t<tc a poorer magnetic performance could be expected for (110) films than

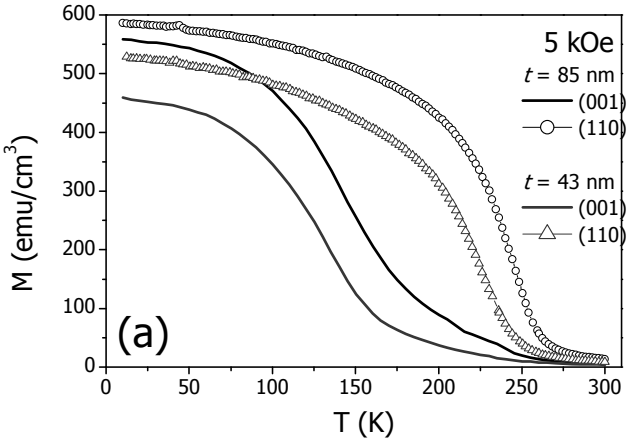

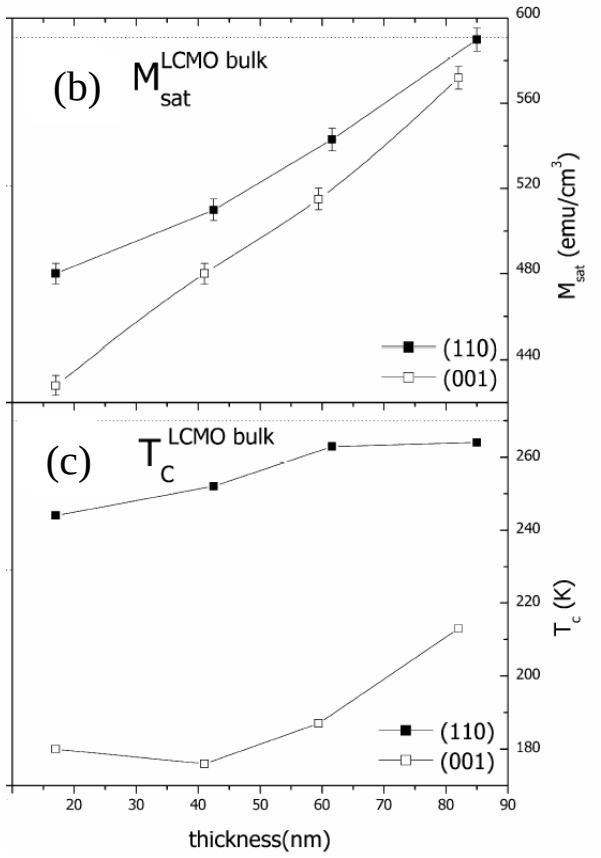

Fig. 12. Magnetisation as a function of T (a) and magnetization saturation (b) and Curie temperature (c) as a function of layer orientation and thickness

for (001) films, according to our EELS results, where a greater La-rich dead magnetic layer and a greater phase separation have been found for (110) films. At the moment TEM and EELS characterization is being carried out on thicker films, in parallel with the measurement of the magnetic properties of very thin layers, in order to confirm these assumptions by cross-correlation. As a preliminary result, the EELS analysis of a LCMO layer of thickness t=84 nm grown on (110) STO substrate does not reveal any evidence of Mn valence state modification across the whole layer, in good agreement then with magnetic data included in figure 12.

V. CONCLUSION

In the present work we have analyzed the microstructure of LCMO/LAO samples prepared by RF-sputtering in concomitance with their magnetic properties. The existence of a cationic segregation process of La^{3+} ions towards the surface of the film has been detected. This segregation process is more important in thin as grown samples and is considerably reduced after annealing samples in air at high temperature. In parallel with this, samples exhibit depressed magnetic properties that substantially improve after annealing. La segregation would imply a departure from the nominal composition (2/3-1/3) $Mn^{3+/4+}$ valence valance thus, becoming an efficient mechanism for the reduction of T_C and M_S. High temperature annealing processes would promote a rediffusion of La ions helping in recovering the nominal $Mn^{3+/4+}$ valence balance, thus improving the magnetic properties. Whereas depressed magnetic performances of LCMO thin films grown on LAO substrates had been usually explained in terms of the presence of microstructural defects, in the present work we have shown that La^{3+} cationic diffusion may play a major role in the observed degradation of the magnetic performances.

On the other hand, we have also shown the comparative results of simultaneous growth by RF-sputtering of thin LCMO layers on (001) and (110) STO substrates. EELS analysis has detected a La migration towards free surface, which is a surprising result that seems to be characteristic of very thin films, and is more pronounced for the (110) orientation. XRD experiments have also yielded anomalous lattice parameter and unit cell volume results for very thin films, especially for the (110) orientation. Thus, an anomalous low thickness t<tc regime of LCMO films grown on STO as a function of its orientation has been identified. In order to better understand it, further work on cation migration analysis depending on the layer thickness and the correlation with cell volume variation, strain conditions and magnetic behaviour is now in progress.

REFERENCES

[1] J. S. Moodera and G. Mathon, J. Magn. Magn. Mater., 200, 248 (1999)
[2] S. S. P. Parkin, K. P. Roche, M. G. Samant, P. M. Rice, R. B. Byers, R. E.Scheuerlein, E. J. O'Sullivan, S. L. Brown J. Bucchigano, D. W. Abraham,Yu Lu, M. Rooks, P. L. Trouilloud, R. A. Wanner, and W. J. Gallagher, J. Appl. Phys., 85, 5828 (1999)
[3]J. Simon T. Walther, W. Mader, J. Klein, D. Reisinger, L. Alff,, R. Gross, App. Phys. Lett., 84, 3882 (2004)
[4]F. Pailloux, D. Imhoff, T. Sikora, A. Barthélémy, J.-L. Maurice, J.-P. Contour, C. Colliex and A. Fert, Phys.Rev. B 66, 14417 (2002)
[5]E. Gommert, H. Cerva, J. Wecker, K. Samwer, J.App.Phys. 85, 5417 (1999)
[6] J. Fontcuberta, I.C. Infante, V. Laukhin, F. Sánchez, M. Wojcik, E. Jedryka, J. App.Phys. 99, 8A701 (2006)
[7] K. Daoudi, T. Tsuchiya, I. Yamaguchi, T. Manabe, S. Mizuta, T. Kumagai J.App.Phys. 98, 013507 (2005)
[8] Egerton, R. F. Electron Energy loss Spectroscopy in the Electron Mycroscope, Plenum Press, 1996
[9] Verbeek, J. Ph.D. Thesis, Antwerpen, 2002
[10] S. Estradé, Ll. Abad, V. Laukhin, Ll. Balcells, B. Martínez, J. Arbiol, F. Peiró, App. Phys. Lett., submitted 2007
[11] V. Potin, E. Hahn, A. Rosenauer, D. Gerthsen, B. Kuhn, F. Scholz, A. Dussaignec, B. Damilano, N. Grandjean, J. Cryst. Growth 262, 145 (2004)
[12] T. Riedl, T. Gemming, K. Wetzig, Ultramicroscopy 106, 284 (2006)
[13] Y.Q. Wang, X.F. Duan, Z.H. Wang, B.G. Shen, Materials Science and Engineering A 333, 80 (2002)
[14] Z.L. Wang, J. Bentley, N.D. Evans, Micron 31, 355 (2000)
[15] Z.L. Wang, J.S. Yin and Y.D. Jiang, Micron 31, 571 (2000)
[16] H. Kurata and C. Colliex, Phys.Rev. B 48, 2102 (1993)
[17] V. Marchetti, J. Ghanbaja, P. Gérardin and B. Loubinoux, Holzforschung 54, 553 (2000)
[18] DEA Thesis from LL.Abad, Institute of Materials Science, ICMAB-CSIC
[19] A. Biswas, M. Rajeswari, R.C. Srivastava, Y.H. Li, T. Venkatesan, R.L. Greene and A.J. Millis. Phys. Rev. B 61, 9665 (2000)
[20] X.J. Chen, H.U. Habermeier, H. Zhang, G. Gu, M. Varela, J. Santamaria and C.C. Almasan. Phys. Rev. B-72, 104403 (2005)
[21] Ll. Abad, B. Martinez and Ll. Balcells. Appl. Phys. Lett. 87, 212502 (2005)
[22] I. C. Infante, F. Sánchez, J. Fontcuberta, S. Fusil, K. Bouzehouane, G. Herranz, A. Barthélémy, S. Estradé, J. Arbiol, F. Peiró, R. J. O. Mossanek, M. Abbate, M. Wojcik, J. App. Phys., 101, 093902 (2007)
[23] DEA Thesis from I.C. Infante, Institute of Materials Science, ICMAB-CSIC
[24] S. Estradé, I.C. Infante, V. Laukhin, F. Sanchez, M. Wojcik, E. Jedryka, J. Arbiol, F. Peiró, App. Phys. Lett., submitted 2007
[25] J.L. Maurice, F. Pailloux, A.Barthélémy, O. Durand, D. Imhoff, R. Lyonnet, A. Rocher and J.P. Contour, Phyl. Mag. 83, 3201 (2003)